GDCh Research Article Angewandte International Edition Chemie www.angewandte.org

How to cite: *Angew. Chem. Int. Ed.* **2025**, *64*, e202510412
doi.org/10.1002/anie.202510412

Biochemistry Very Important Paper

Designing New Natural-Mimetic Phosphatidic Acid: A Versatile and Innovative Synthetic Strategy for Glycerophospholipid Research

Antoine Schlichter[+], Alexander Wolf[+], Thomas Ferrand[+], Aurelien Cocq[+], Lina Riachy[+], Steven Vertueux[+], Brice Beauvais[+], Marine Courvalet, Paul-Joël Henry, Emeline Tanguy, Louis Gonzales, Rémy Ferlet, Fanny Laguerre, Charles Decraene, Alexia Pellissier, Muriel Sebban, Cyrille Sabot, Lydie Jeandel, Sarah Cianférani, Jean-Marc Strub, Magalie Bénard, Victor Flon, Valérie Peulon-Agasse, Pascal Cardinael, Stéphane Ory, Stéphane Gasman, Pierre-Yves Renard[+], Maïté Montero-Hadjadje[+],* Nicolas Vitale[+],* and Sébastien Balieu[+]**

Abstract: Glycerophospholipids (GPLs) play important roles in cellular compartmentalization and signaling. Among them, phosphatidic acids (PA) exist as many distinct species depending on acyl chain composition, each one potentially displaying unique signaling function. Although the signaling functions of PA have already been demonstrated in multiple cellular processes, the specific roles of individual PA species remain obscure due to a lack of appropriate tools. Indeed, current synthetic PA analogues fail to preserve all the functions of natural PA. To circumvent these limitations, we developed a novel synthetic approach to produce PA analogues without compromising structural integrity of acyl chains. Moreover, addition of a clickable moiety allowed flexible grafting of different molecules to PA analogues for various biological applications. Hence, this innovation also provides powerful tools to investigate specific biological activities of individual PA species, with potential applications in unraveling complex GPL-mediated signaling pathways.

Introduction

Lipids are essential constituent of organisms, yet their extreme diversity and lack of appropriate tools overcomplicate their studies.[1,2] Glycerophospholipids (GPLs) are a subclass of lipids, constituting the bulk of cellular membranes, but are also able to perform important signaling functions within cells. Coexistence of hundreds of GPLs within biological membranes suggests that each plays major, yet potentially, non-overlapping roles. Furthermore, given their rapid and complex metabolism, establishing the roles of an individual lipid, in a spatial and temporal resolved manner, remains challenging.[3] Among GPLs, phosphatidic acids (PA), composed of a single phosphomonoester headgroup (the smallest headgroup within GPL), have been shown to exhibit structural diversity within cells based on their fatty acyl chains composition.[4,5] PA has attracted considerable attention and has been proposed to play pivotal roles in

[*] Dr. A. Schlichter[+], Dr. A. Cocq[+], Dr. S. Vertueux[+], B. Beauvais[+], P.-J. Henry, Dr. L. Gonzales, Dr. R. Ferlet, A. Pellissier, Dr. M. Sebban, Dr. C. Sabot, Prof. P.-Y. Renard[+], Dr. S. Balieu[+]
Univ Rouen Normandie, INSA Rouen Normandie, CNRS, Univ Caen Normandie, ENSICAEN, Normandie Univ, CARMeN UMR 6064, INC3M FR 3038, Rouen F-76000, France
E-mail: pierre-yves.renard@univ-rouen.fr
sebastien.balieu@univ-rouen.fr

Dr. A. Wolf[+], Dr. E. Tanguy, Dr. C. Decraene, Dr. S. Ory, Dr. S. Gasman, Dr. N. Vitale[+]
Centre National de la Recherche Scientifique, Institut des Neurosciences Cellulaires et Intégratives, Université de Strasbourg, Strasbourg, France
E-mail: vitalen@unistra.fr

T. Ferrand[+], Dr. L. Riachy[+], M. Courvalet, Dr. F. Laguerre, Dr. L. Jeandel, Prof. M. Montero-Hadjadje[+]
INSERM, Normandie Univ, U1239, Laboratoire de Différenciation et Communication Neuroendocrine, Endocrine et Germinale, Institut de Recherche et d'Innovation Biomédicale de Normandie, Univ Rouen Normandie, Rouen 76000, France
E-mail: maite.montero@univ-rouen.fr

Dr. S. Cianférani, Dr. J.-M. Strub
Laboratoire de Spectrométrie de Masse BioOrganique, IPHC UMR 7178, CNRS, France and Infrastructure Nationale de Protéomique ProFI–UAR2048, Université de Strasbourg, Strasbourg 67037, France

Dr. M. Bénard
INSERM, CNRS, Normandie Univ, UMR, HeRaCleS, Institut de Recherche et d'Innovation Biomédicale de Normandie, Univ Rouen Normandie, Rouen 76000, France

Dr. V. Flon, Dr. V. Peulon-Agasse, Prof. P. Cardinael
Laboratoire Sciences et Méthodes Séparatives SMS, Univ Rouen Normandie, FR3038, UR 3233, Rouen F-76000, France

[+] These authors contributed equally to this work

Additional supporting information can be found online in the Supporting Information section

© 2025 The Author(s). Angewandte Chemie International Edition published by Wiley-VCH GmbH. This is an open access article under the terms of the Creative Commons Attribution-NonCommercial-NoDerivs License, which permits use and distribution in any medium, provided the original work is properly cited, the use is non-commercial and no modifications or adaptations are made.

 © 2025 The Author(s). Angewandte Chemie International Edition published by Wiley-VCH GmbH

multiple cellular functions.[3,4] Accordingly dysregulation of its metabolism is linked to numerous diseases including neurodegeneration,[6] intellectual disabilities,[7,8] cancer,[9] fragile X,[10] and Coffrin–Lowry syndromes.[11] Supporting these multiple signaling functions is the complex interconnected metabolic pathways leading to PA synthesis and metabolism allowing cell to precisely control PA levels in the different membrane compartments. Three alternative pathways allow the biosynthesis of signaling PA including i) the phosphorylation of diacylglycerol (DAG) by DAG-kinases, ii) the acylation of lyso-PA by lyso-PA-acyltransferase enzymes and iii) the hydrolysis of the distal phosphodiester bond in phospholipids by phospholipases D (PLD). Recent crystal structure of PLD further provided insight into the isoform selectivity[12] and regulation by Rho guanosine triphosphatases (GTPases) and phosphatidylinositol 4,5-bisphosphate (PI(4,5)P2).[13] The small anionic phosphate headgroup provides to PA a combination of unique cone shaped geometry and negative charge.[7] At the molecular level, these two characteristics allow PA to interact with various proteins to modulate their catalytic activity and/or their membrane association and also affect membrane geometry by creating local negative curvatures.[14] To date more than 50 different proteins were identified as direct interactor of PA including various GTPases such as rapidly accelerated fibrosarcoma (Raf),[15] protein kinases such as mammalian target of rapamycin complex (mTORC),[16] and ion channel such as TWIK-Related Acid-sensitive Autonomous K^+ (TRAAK) channel,[17] but neither the cell state nor the exact species of PA (fatty acyl chains composition) involved in the interaction have been taken into account, thus interaction accuracy and precise role remain elusive. Accordingly, accurate chemobiology tools are required to shade light on the biological relevance of these interactions are required.

Currently available GPL analogues,[18] aiming at understanding their individual role, rely on modified fatty acyl chains (with fluorophore,[19] photo-crosslinker[20] or a clickable moiety[21]), or modified headgroups, which is not applicable to PA. However, side chains composition is critical for biological activity of GPLs and altering them impacts their functions.[22–25]To preserve biological properties of GPLs, it is anticipated that both their headgroups and fatty acyl chains[26] must remain unchanged. Hence, the glycerol backbone might be the most relevant place to introduce chemobiological modifications. This approach was first proposed by adding a clickable azidomethyl moiety on the glycerol core.[27] In vitro studies demonstrated that this modification had little effect on PA probe association with protein kinase C (PKC), validating this strategy. However, the proposed synthesis only allowed grafting two identical fatty acyl chains, which does not match the diversity of natural GPLs. To circumvent these limitations, we developed a novel synthetic strategy for clickable azide-based GPL analogues (GPL-N3), allowing to keep untouched fatty acyl chain composition and phosphate head group, thus mimic natural GPL species, and first applied this strategy to PA, where phosphate headgroup modification is not applicable. The specificity of those novel PA analogues was validated in chromaffin cells, a model in which we recently demonstrated that different PA species have exclusive non-redundant functions in the secretory pathway and allowed confirmation of previously identified PA-interacting proteins involved in this process but also unveiled dozens of new potential PA binding partners.

Results and Discussion

Convergent Synthesis of GPL-N3 and GPL Probes

We developed a new specific synthetic route to achieve regio-selective and stereo-specific grafting of fatty acyl chains. This method incorporates a clickable moiety on the glycerol core of GPL structure (Figure 1). Headgroup protection as dimethylphosphoester facilitated purifications steps of various intermediates. To obtain accurate stereochemistry of the stereospecific numbering (*sn)*-2 position, synthesis was initiated with dimethyl-L-tartrate. Several transformations allowed us to differentiate the four carbon atoms of the tartric backbone resulting in intermediate **8**, the common building block for all GPL-N_3.

The *sn*-3 position was functionalized with dimethyl phosphate ester, the *sn*-2 was protected with a *p*-methoxylbenzyl (PMB) group, and the *sn*-1 position was let free. The additional carbon on the glycerol core, designated as *sn*-0, was equipped with an azide moiety. Despite high yields of the first synthetic steps (Figure 1a and Supporting Information 1.5.1), an unexpected deprotection of the phosphate ester occurred during the nucleophilic substitution of tosylate **7** by sodium azide leading to **9**. Although reaction between lithium azide, and to a lesser extent sodium azide, is well known for cleaving methyl phosphate monoesters,[28] it was expected that tosylate displacement by an azide would be selective over this ester cleavage. However, this was not the case despite modifications in temperature, number of equivalents, azide source, solvents, and leaving groups tested. The optimal solution found was to realkylate the deprotected phosphate of **9** using $TMSCHN_2$[29] giving **8** in an overall 14% yield in seven steps (Figure 1a). Using this synthetic route, **8** could be obtained at the gram scale.

The second part of the synthetic route afforded four different PA-N_3 **13a-d** from the common building block **8,** with regio-selective addition of desired fatty acids through sequential acylation/deprotection/acylation steps. The *sn*-1 position was acylated with a saturated fatty acid (stearic acid), leading to ester **10** with good yield thanks to the coupling reagent DCC/DMAP. Subsequent deprotection of PMB moiety was carefully monitored in mild conditions by ^{31}P NMR until completion, immediately followed, without purification, by a second acylation reaction with an unsaturated fatty acid with the same coupling agent DCC/DMAP. This reaction converted resulting *sn*-2 alcohol into esters **12a-d** as quickly as possible avoiding any significant intramolecular trans-esterification reaction with stearate. Velocity of this side-reaction was studied by NMR with shorter fatty acids chains and was well characterized. Thus, in our reaction conditions (0 °C, 5 h or room temperature, 1 h) we avoided this side-reaction and consequently maintained regioselectivity higher than 95% during grafting of fatty

 © 2025 The Author(s). Angewandte Chemie International Edition published by Wiley-VCH GmbH

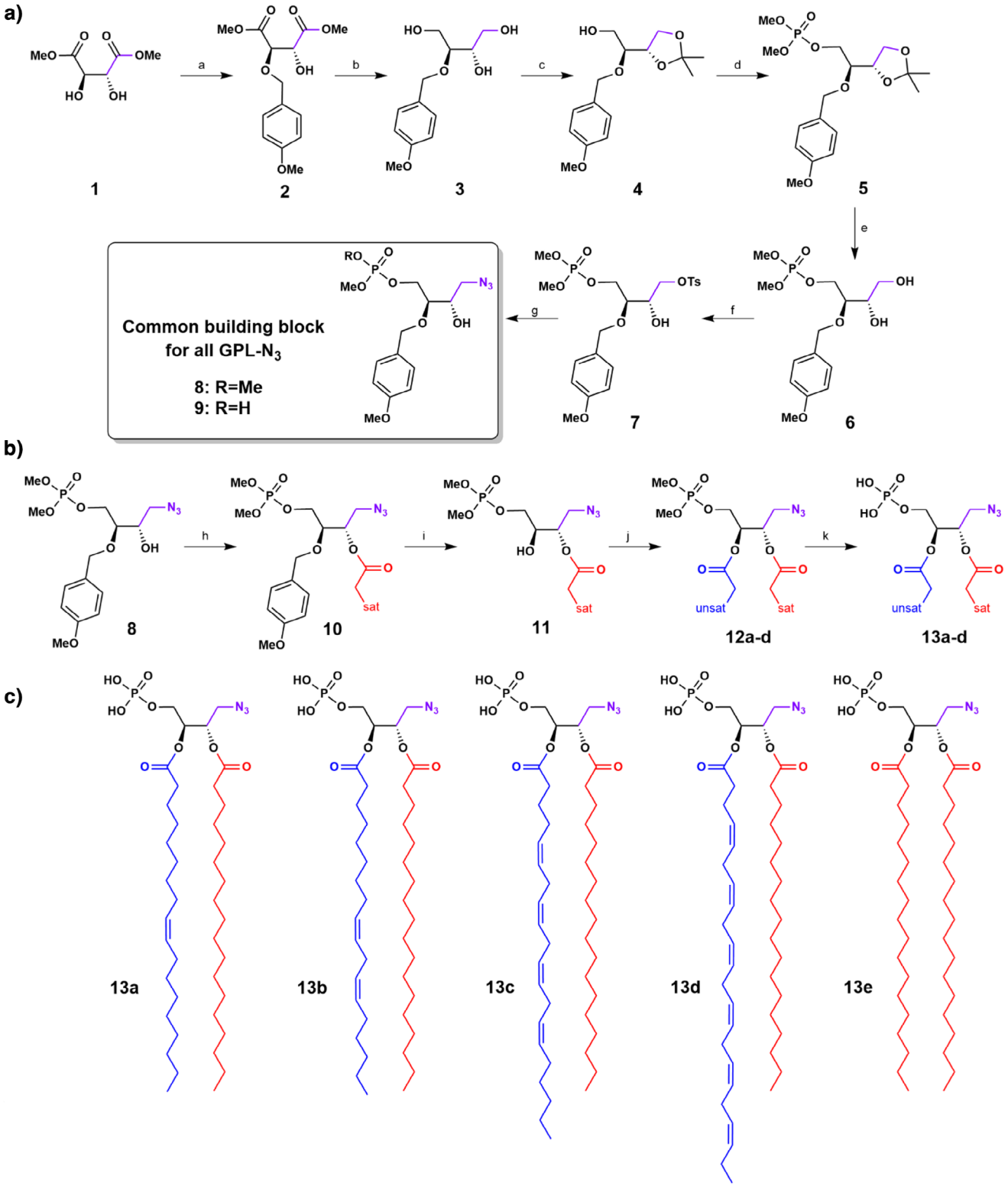

Figure 1. Synthetic route to the common building block 8 leading to PA-N_3 13a-d. a) formal synthesis of the common building block **8** having all the sn positions differentiated. a) PMBBr, Bu_2SnO, Bu_4NI, CsF, Toluene, 70%. b) $NaBH_4$, i-PrOH, 90%. c) 2,2-Dimethoxypropane, APTS, acetone, 70%. d) Dimethylchlorophosphate, t-BuOK, DCM, 76%. e) HCl, MeOH, 85%. f) TsCl, DIPEA, Bu_2SnO (0.5% mol.), toluene, 75%. g) 1) NaN_3, DMF, 2) $TMSCHN_2$, MeOH, 65%. **b**) formal synthesis of four different PA-N_3 **13a–d** from intermediate **8**. h) DCC, DMAP, stearic acid, DCM, 93%. i) DDQ, DCM, PBS buffer (pH = 7.2). j) DCC, DMAP, oleic acid (**12a**), linoleic acid (**12b**), arachidonic acid (**12c**) or docosahexaenoic acid (**12d**), 50% (**12a**, **12b**), 63% (**12c**) 75% (**12d**) over two steps. k) 2-methylbut-2-ene, TMSBr, $CHCl_3$ or 2-methylbut-2-ene, TMSBr, BSTFA, $CHCl_3$, 48 to 95%. **c**) structures of the PA-N_3 (18:0–18:1) **13a**, PA-N_3 (18:0–18:2) **13b**, PA-N_3 (18:0–20:4) **13c**, PA-N_3 (18:0–22:6) **13d** and PA-N_3 (18:0–18:0) **13e**.

© 2025 The Author(s). Angewandte Chemie International Edition published by Wiley-VCH GmbH

acyl chains (see transesterification studies in Supporting Information 1.6). Finally, cleavage of dimethyl phosphate ester of **12a-e** was performed under mild conditions with BSTFA[30,31] and TMSBr to obtain various PA-N_3 **13a-d**, (PA-N_3 (18:0–18:1) **13a,** PA-N_3 (18:0–18:2) **13b**, PA-N_3 (18:0–20:4) **13c**, PA-N_3 (18:0–22:6) **13d**), whereas symmetrical PA-N_3 (18:0–18:0) **13e** was also obtained through a shorter synthetic pathway described in supplementary materials (Figure 1b,c and Supporting Information 1.5.2). This process leading to **13a-d** is amenable to any other fatty acyl chain composition, thus allowing us to accordingly access PA structural diversity.

To produce PA probes from PA-N_3 **13a-d**, we performed strain-promoted azide–alkyne cycloaddition (SPAAC) ligation reaction to avoid generation of reactive oxygen species (ROS) with copper (I)[32]; even though this reaction is slower than copper-catalyzed azide–alkyne cycloaddition (CuAAC),[33] SPAAC has proved to be amenable to in vivo chemistry within life cells. The chosen cyclooctyne SPAAC partners were obtained from dibenzoazacyclooctyne (DIBAC) derivatives offering a good compromise between stability and reactivity. The DIBAC-C_6-Amine synthesis[34] was optimized to minimize side products formation and improve reaction repeatability, especially for the dibromation/elimination sequence leading to the cyclooctyne ring (Supporting Information 1.5.3). Thereafter a coupling reaction with activated carboxylic acid derivatives was performed affording photo-crosslinker (PCL)-DDA1 **18** and DIBAC-C_6-ATTO 647N **19** or S_NAr reaction to get DIBAC-C_6-NBD **20** (Figure 2a). These chemobiological tools were first developed with PA-N_3 (18:0–18:1) **13a** and PA-N_3 (18:0–22:6) **13d** due to their non-overlapping functions in neurosecretion.[35] SPAAC reactions led to six new PA probes bearing either diazirines[36] as photocrosslinkers with PA-DDA1 (18:0–18:1) **21a** and PA-DDA1 (18:0–22:6) **21d** or either fluorophore with PA-NBD (18:0–18:1) **22a**, PA-NBD (18:0–22:6) **22d**, PA-ATTO 647N (18:0–18:1) **23a** and PA-ATTO 647N (18:0–22:6) **23d** (Figure 2b).

Biocompatibility and Membrane Incorporation of Synthetic Mono- and Poly-Unsaturated PA Analogues in Neurosecretory Cells

Exocytosis is the final step of neurosecretion and neurotransmitter release leading to the liberation of the secretory products and has been the topic of intense investigation for decades. The adrenal chromaffin cell model has provided and continues to provide profound insights into the secretory pathway, especially concerning the enigmatic contribution of membrane lipids in exocytosis.[37] Over the last two decades, chromaffin cells have served as an important cellular model using genetic and pharmacological invalidation to demonstrate a key role for phospholipase D1 (PLD1)-generated PA in regulated exocytosis.[38] The current model proposes that PA plays a biophysical role, generating a negative curvature and thus promoting fusion of secretory vesicles with the plasma membrane but also acts on several additional steps along the secretory pathway[39] Lipidomic analysis have revealed that most, if not all, intracellular membrane compartments contain PA with a specific distribution of the different species among these compartments,[40] with high levels of polyunsaturated PA in the secretory granule membranes.[35,41]

Primary chromaffin cell live-imaging revealed that PA-ATTO 647N (18:0–18:1) **23a** and PA-ATTO 647N (18:0–22:6) **23d** analogues rapidly inserted into cellular membranes and accessed intracellular compartments without visible alteration (Figure 3a,b and Supporting Information 2.4 including Video 1–3). PA-ATTO 647N (18:0–22:6) **23d** displayed faster access to the plasma membrane and accumulated more effectively in internal membrane compartments than PA-ATTO 647N (18:0–18:1) **23a**, in agreement with the established cellular gradient of poly-unsaturated GPL, decreasing from intracellular organelles towards the plasma membrane.[42] Validating the rapid access of PA analogues to the inner leaflet of the plasma membrane, the PA sensor Spo20p-GFP[40] was recruited to the plasma membrane within minutes of incubation of PA analogues **13a**, **13d**, **21a,** and **21d** (Figure 3c,d). These data confirm integrity and stability of synthetic PAs *in cellulo*, but also their ability to interact with a known PA binding protein, and highlight their potential utility to study membrane dynamics and signaling processes in live cells.

Functional Validation of Synthetic PA Analogues in the Secretory Process

To functionally validate these new synthetic PA analogues, we tested their ability to participate in membrane remodeling: interaction between chromogranin A (CgA) glycoprotein, and PA (18:0–18:1) being able to induce such membrane remodeling. In presence of CgA-AF633, giant unilamellar vesicles (GUVs) containing PA-NBD (18:0–18:1) **22a** exhibited significant budding events in agreement with what was previously observed.[41] As expected, fluorescence microscopy images showed colocalization of both partners. In contrast, CgA-AF633 failed to induce the budding of GUVs containing commercially available PA (18:1–6:0-NBD) bearing a modification on fatty acyl chains probably because the modified acyl chain loop up to the surface of the vesicle.[43] (Figure 4a). Quantitative analysis confirmed that in presence of CgA we observed significantly more budding GUVs when they were formed with PA-NBD (18:0–18:1) **22a** than with PA (18:1–6:0-NBD) (Figure 4b), demonstrating that *(i)* CgA interacts effectively with synthetic PA-NBD (18:0–18:1) analogue **22a**, and *(ii)* this interaction is functional, inducing membrane remodeling and vesicle budding, mimicking cellular properties of native PA (18:0–18:1) in Golgi and secretory granule membranes. Conversely, commercial PA (18:1–6:0-NBD) failed to replicate those effects.

The activation of the mTOR pathway represents one of the best characterized signal pathways regulated by intracellular PA levels. Hence, we used the phosphorylation of mTOR, ERK, and RS6K as a readout and found that the different synthetic PA activated the mTOR pathway as effectively as the native PAs validating their functionality (FigureSI 16).

PA synthesized by phospholipase D (PLD) promotes secretion from various cell types including neurons,

 © 2025 The Author(s). Angewandte Chemie International Edition published by Wiley-VCH GmbH

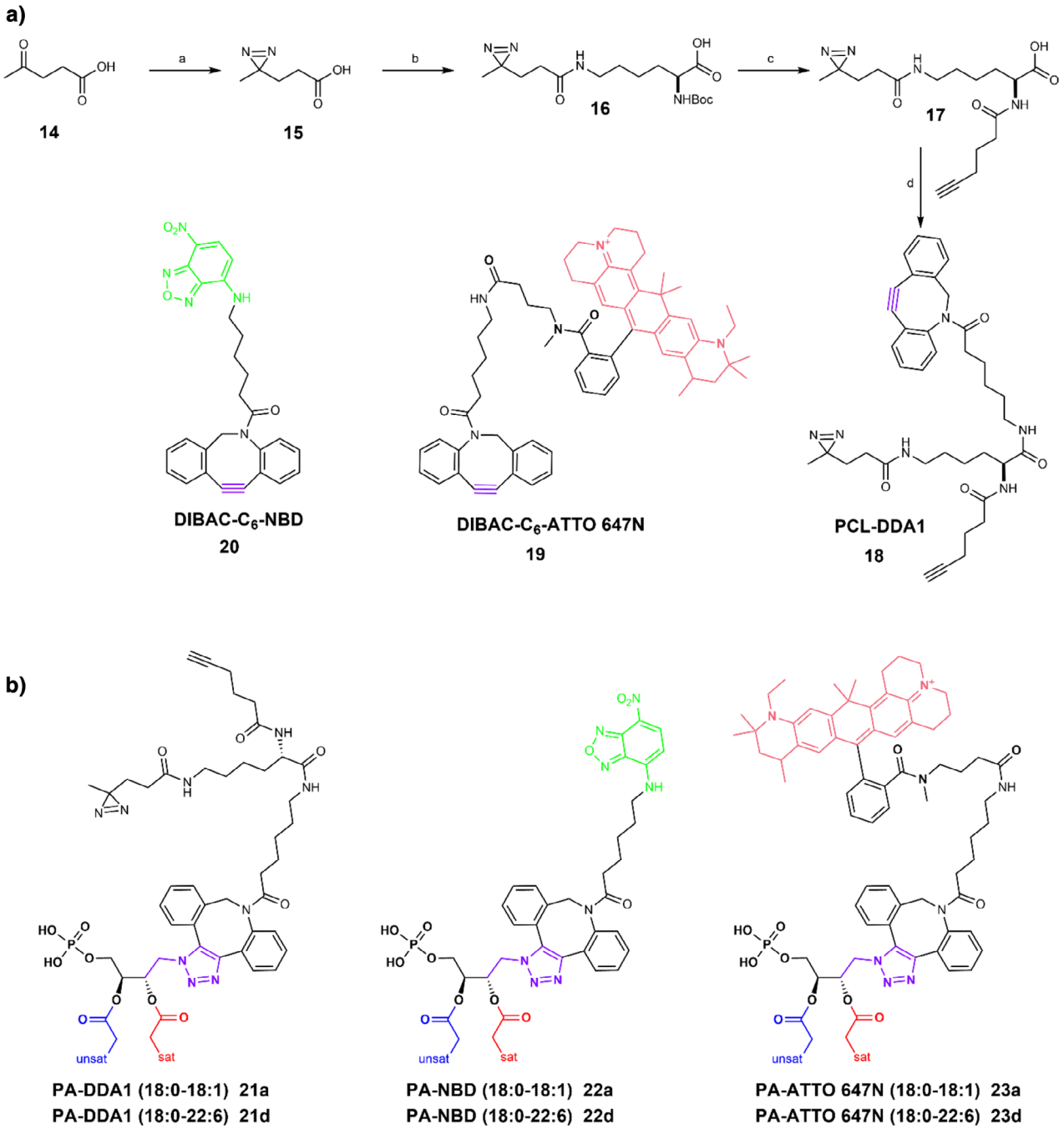

Figure 2. Synthesis of the PA analogues. a) formal synthesis of the PCL-DDA1 **18** and structure of the synthesized clickable fluorophore DIBAC-C_6-ATTO 647N **19** and DIBAC-C_6-NBD **20**. a) 1) NH_3, MeOH, t-BuOCl, 2) t-BuOCl b) 1) NHS, EDCI, DMF, 2) Boc-Lys-OH, DIPEA, DMF, 80%. c) 1) TFA, DCM, 2) Pent-5-yn-N-hydroxysuccinimide ester, 50% over two steps. d) 1) NHS, EDCI, THF, 2) DIBAC-NH_2, DIPEA, rt, 20% over two steps. **b**) structures of the PA probes **21–23** obtained by SPAAC click-chemistry between cyclooctynes **18–20** and PA-N_3 **13a** and **13d**.

endocrine, and exocrine cells.[39,44,45] For instance, we previously reported that knock out, knock-down, or pharmacological inhibition of phospholipase D1 (PLD1) impaired catecholamine release from chromaffin cells by altering multiple steps of the neurosecretory process.[35,40] Lipidomic analysis previously revealed that PA levels were reduced by about 50% in mouse PLD1 KO cells.[40] PLD1 inhibitors such 5-Fluoro-2-indolyl des-chlorohalopemide (FIPI) and Cayman chemical (CAY)93 fully recapitulated this effect and inhibited exocytosis as potently as PLD1 KO, supporting the notion that these inhibitors effectively PA synthesis in response to chromaffin cell stimulation.[40] Interestingly, extracellular provision of mono-unsaturated PA (18:0–18:1) restored the number of exocytotic events, whereas extracellular provision of poly-unsaturated PA (18:0–22:6) regulated the kinetics of individual events. Hence, to assess whether synthetic PAs recapitulate these specific biological effects, we used DβH labeling of exocytotic spots

 © 2025 The Author(s). Angewandte Chemie International Edition published by Wiley-VCH GmbH

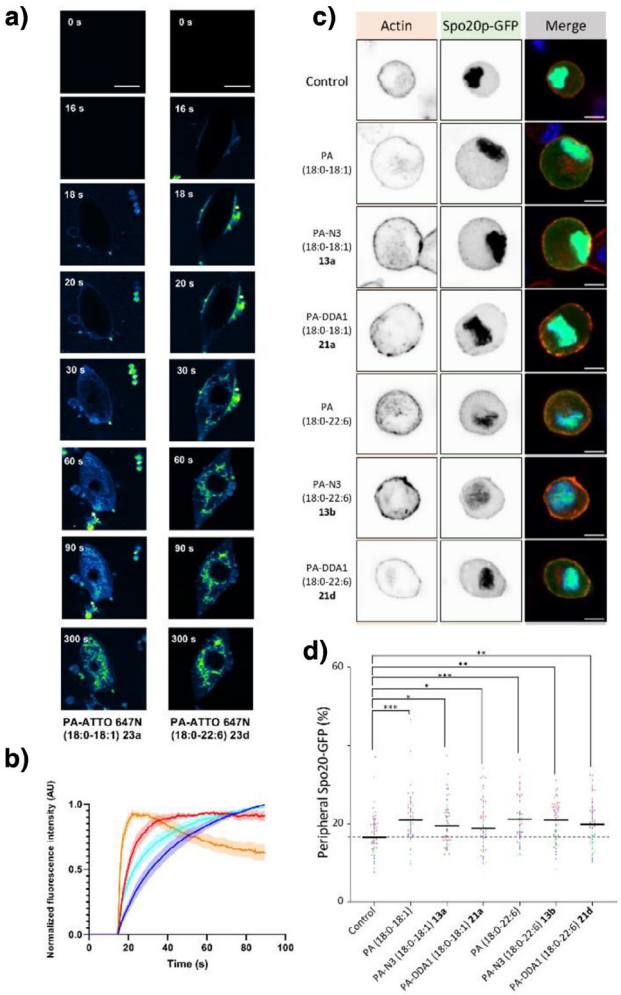

Figure 3. Membrane incorporation of synthetic PA analogues. a) Live-cell imaging showing the incorporation kinetics of 3 μM fluorogenic PA-ATTO 647N (18:0–18:1) **23a** or PA-ATTO 647N (18:0–22:6) **23d** on bovine chromaffin cells. Images have been false colored with ImageJ's Green Fire Blue LUT (intensity: blue < green < yellow). Biomolecules have been added on living cells 15 s after the beginning of recording (arrow on graph). Images were acquired at a speed of 2 frames per second for 90 s. Scale bar, 10 μm. b) Mean fluorescence intensity was analyzed in the whole cell (dark blue line: **23a**; light blue line: **23d**) and in a peripheric area of 500 nm width (red line: **23a**; orange line: **23d**). AU, arbitrary units. The maximum fluorescence intensity was normalized to 1. Analysis was performed on 6 cells from 4 independent cell cultures. Data are expressed as mean ± SEM.; c) Recruitment of the PA sensor Spo20p-GFP after addition of 100 μM natural PA or synthetic PA analogues. Bovine chromaffin cells overexpressing the PA sensor Spo20p-GFP were incubated with the mentioned natural PAs or synthetic PA analogues for 15 min prior to fixation. Representative confocal images are shown, with phalloidin-Atto647N (Actin) and Spo20p-GFP (PA sensor) channel displayed individually as an inverted grayscale image and merged (Blue: nucleus, red: actin and green: Spo20p-GFP). Scale bar, 5 μm. d) quantification of plasma membrane recruitment of PA sensor Spo20p-GFP. Data are represented as median, and each point is a measure from an individual cell. Points are colored coded (red, blue, green, or magenta) according to experimental repeats. Basal recruitment of Spo20p-GFP is indicated by the dotted line. *: $p < 0.05$, **: $p < 0.01$, ***: $p < 0.001$, Kruskall–Wallis followed by Dunn's multiple comparisons test versus control ($N = 60$ per condition, 15 cells from four experimental repeats performed on two independent cultures).

combined with amperometric measurements as reporters of the secretory activity of chromaffin cells. Potent inhibition of DβH staining induced by the PLD1 inhibitor CAY93 was efficiently rescued by synthetic PA (18:0–18:1) whether they harbored a N_3-linker **13a**, a fluorescent 7-Nitrobenz-2-oxa-1,3-diazole (NBD) group **22a**, or a PCL DDA1 moiety **21a** (Figure 5a,b). Importantly, synthetic PAN_3 (18:0–22:6) **13d** and its derived DDA1 probe **21d** failed to rescue DβH labeling back to the control condition, in agreement with data obtained with natural PA (18:0–22:6). Moreover, addition of acyl chain modified PA (16:0–6:0-NBD) was also unable to rescue the effects of PLD1 inhibition (Figure 5a,b). Furthermore, electrochemical recording of catecholamine secretion on PLD1 inhibited chromaffin cells enabled us to explore the specific contribution of PA (18:0–22:6) and PA-DDA1 (18:0–22:6) **21d**. CAY93 treatment reduced the number of measured exocytotic events, an effect that was not rescued by addition of natural and synthetic poly-unsaturated PA species (Figure 5c–f,h). However, CAY93 also slowed down the speed of individual fusion events (Figure 5 g,i) and increased the duration of individual fusion pores (Figure 5j). Both those effects were effectively rescued by PA (18:0–22:6) and PA-DDA1 (18:0–22:6) **21d**. Hence, the synthetic PA analogues developed recapitulate exclusive functions of natural mono- and poly-unsaturated forms of PA during neuroendocrine secretion, a capability not observed with PA (18:0–6:0-NBD). These data strongly support the idea that modifications targeting the glycerol backbone of PA do not alter functional properties of these PA analogues within cells.

Characterization of the PA Interactome in Neurosecretory Cells Using Synthetic PA-DDA1

To further assess functional differences between mono- and polyunsaturated PA, we performed photo-crosslinking experiments to map the various PA interacting proteins landscape during neurosecretion. Chromaffin cells were incubated with PA-DDA1 (18:0–18:1) **21a** or PA-DDA1 (18:0–22:6) **21d** and illuminated to crosslink PA interactants in resting, stimulated, or post-stimulation states or without illumination. Synthetic PAs were then purified from cell lysates using the alkyne moiety of DDA1 by performing a CuAAC reaction with azide tagged beads. Finally, interacting proteins were identified by mass spectrometry following trypsin digestion of the purified samples. A total of 1264 polypeptides identified without illumination were considered as background. After subtracting them, we identified 778 potential direct or indirect PA partners. Validating our strategy, these include proteins previously identified as PA interactants in assays using cell extracts incubated with PA coupled to agarose beads[46,47] and known PA interactants validated biochemically.[14,48–50] (TableSI 3). Additionally, many novel potential PA partners were discovered. Among these, 286 were specific to PA (18:0–18:1) **21a** and 341 to PA (18:0–22:6) **21d**, whereas 151 were common to both PA species (Figure 6a). Furthermore, some of these interactants were specific to either resting, stimulated, or post-stimulated cells, whereas others were present in two or

 © 2025 The Author(s). Angewandte Chemie International Edition published by Wiley-VCH GmbH

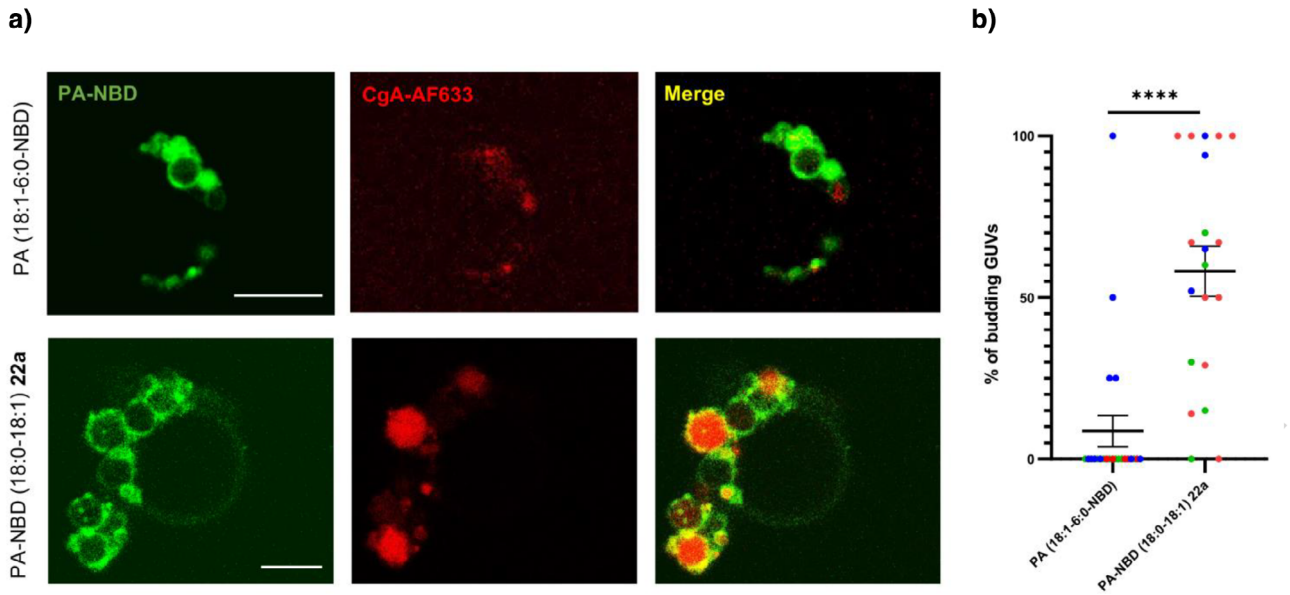

Figure 4. Liposome-based evaluation of synthetic fluorescent PA-NBD analogues. a) representative pictures of GUVs composed of 96% DOPC and 4% PA (18:1–6:0-NBD) or 4% PA-NBD (18:0–18:1) **22a**, in the presence of CgA-AF633. Scale bar, 10 µm. b) quantification of budding GUVs composed of 96% DOPC and 4% PA (18:1–6:0-NBD) or 4% PA-NBD (18:0–18:1) **22a** with CgA-AF633. Each point represents the result of GUV analysis from three independent experiments (20 and 22 images for each type of PA-NBD containing-GUVs, respectively). Points are colored coded (red, blue, or green) according to experimental repeats. ****: $p < 0.0001$, Mann Whitney test.

three conditions (Figure 6a), highlighting the dynamic nature of these interactions.

Gene ontology (GO) analysis classifying proteins based on molecular function, biological process, and cellular component revealed specific enrichments in proteins associated with membrane organelles and trafficking pathways. Notably, we observed clear differences between PA species (Figure 6b and FigureSI 19). Furthermore, although potential partners of PA (18:0–18:1) were less abundant, they showed a more distinct pattern across the three cellular states tested, with a dramatic increase in response to stimulation (Figure 6b and Figure SI 21).

The potential PA partners inferred to the GO terms "cellular components" were pooled and search tool for the retrieval of interacting genes/proteins (STRING) maps were generated to visualize the interaction networks (Figure 6c). Interestingly, CgA, known for its role in secretory granule biogenesis through its interaction with PA,[41] was found to interact with both synthetic PA **21a** and **21d** across all conditions (Figure 6c, boxed in black). For PA (18:0–18:1) **21a** an increase in the number of potential partners was observed after stimulation, including proteins related to the vacuolar ATPase (V-ATPase), which has been implicated in PA formation near exocytotic site.[51] (Figure 4c). Additionally, Soluble NSF Attachment REceptor (SNARE)-related proteins were detected specifically for PA-DDA1 (18:0–22:6) **21d** (Figure 6c) in the stimulated condition, consistent with previous observations that PA may interact with syntaxin-1A[52] Of interest, adaptor and membrane coat-related proteins were also detected post-stimulation, possibly related to recycling of granular content by compensatory endocytosis. Several lipid transport proteins were also detected among the potential PA interactants in line with the rapid incorporation of the PA-ATTO 647N in different intracellular compartments (Figure 3a). Both observations suggest that PA may in the majority transit between intracellular membranes through membrane contact sites rather than through vesicular trafficking. Finally, translation-related factors were also identified in the PA interactome, which is in line with the observation that PLD1-derived PA promotes the binding of nuclear factor kappa-light-chain-enhancer of activated B cells (NFκB) or hypoxia-inducible factor 1-alpha (HIF-1α) to the promoters of its target genes increasing the expression of proinflammatory mediators, migration, and angiogenic factors, but to the suppression of the expression of cell cycle arrest genes via inhibition of Forkhead box O3a (FoxO3a) transactivation.[53]

Of note, the newly identified potential partners could be direct or indirect interactors. Thus, direct interaction remains to be probed directly using biochemical approaches. Furthermore, detailed bioinformatic analysis of these protein sequences will provide more information to define PA binding motifs and could lead to identify a minimal PA-binding motif, which has been difficult to define precisely.[43]

To our knowledge, this study represents the first example of GPL-protein interatomic, or "fishing" experiment performed with GPLs embedded in membranes from primary living cells under different physiological conditions. Among the many novel interactants identified, several interesting candidates are involved in lipid transfer, metabolism, and translation highlighting new potential avenues for research. The development of structurally faithful, clickable PA analogues opens new avenues for dissecting the specific roles of individual PA species in disease models and fundamental

 © 2025 The Author(s). Angewandte Chemie International Edition published by Wiley-VCH GmbH

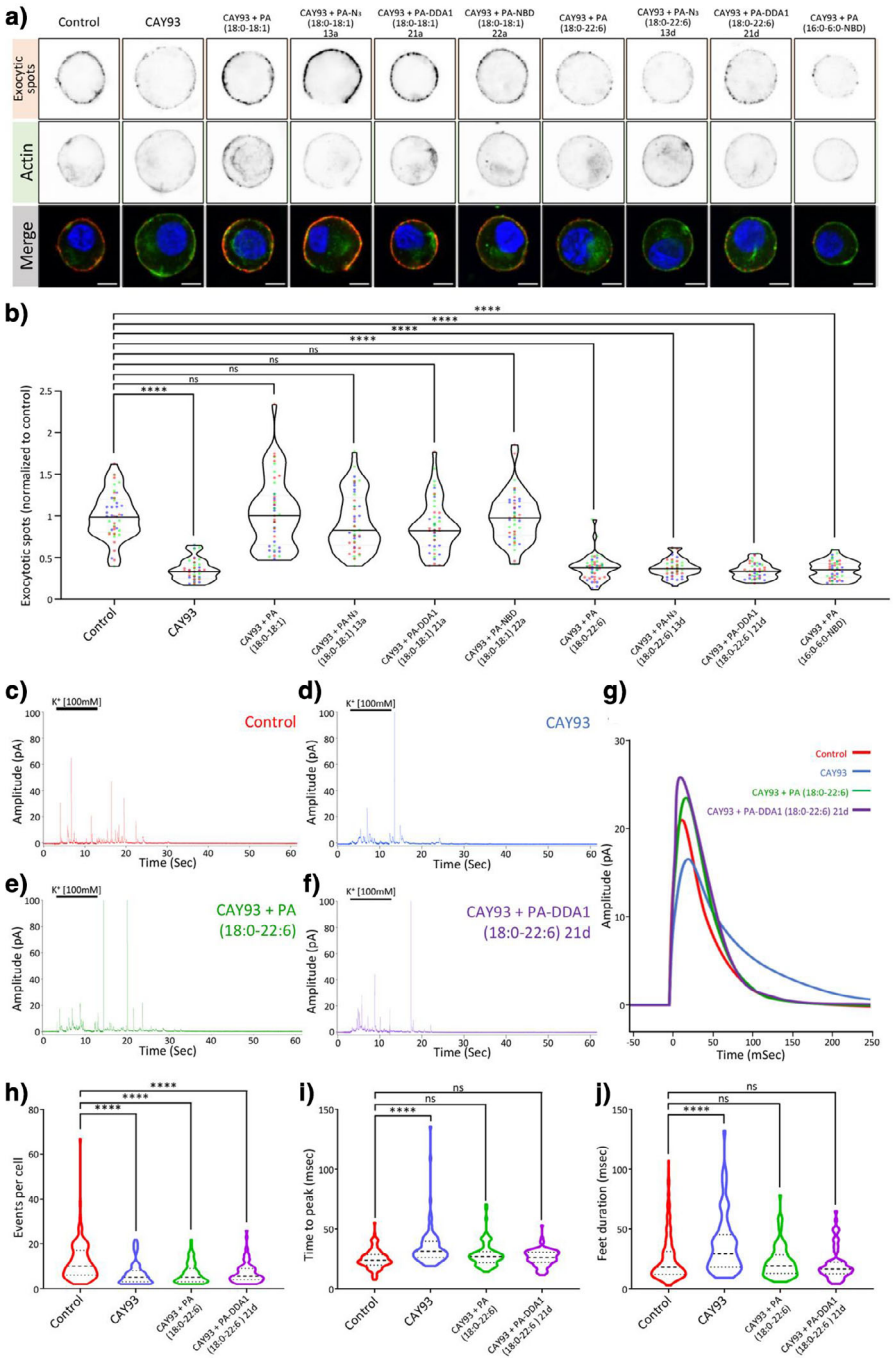

Figure 5. Synthetic PA analogues fully recapitulate the functions of natural PA in neuroendocrine secretion. a) representative confocal images of stimulated bovine chromaffin cells after exocytotic spots staining. PLD1 activity was inhibited with 50 nM CAY93, and cells were incubated with natural PAs and synthetic PA analogues. Exocytotic spot (DβH staining) and actin network (phalloidin-Atto647N staining) are displayed individually as an inverted grayscale image and merged (Blue: nucleus, red: exocytotic spots and green: actin). Scale bar, 5 µm; b) exocytotic spots quantification (DβH staining). Peripheral exocytotic spot intensity has been normalized with the mean control condition of the individual experimental repeat. Data are represented as violins with a straight line at the mean, and each point is a measure from an individual cell. Symbols are colored coded (red, blue, green, or magenta) according to experimental repeats. ns: non-significant, ****: $p < 0.0001$, Kruskall–Wallis followed by Dunn's multiple comparisons test ($N = 45$ per condition, 15 cells from three independent cultures). Without PLD1 inhibition PA addition does not affect overall secretion of cells upon stimulation and specific effects of PA (18:0–22:6) were also reproduced in resting condition (FigureSI 17a). Cell area was not affected by any of the treatments (FigureSI 17b). c)–f) examples of amperometrical traces from cells incubated with or without PLD1 inhibitor (50 nM CAY93) and the mentioned PA species, or PA analogue. Cells were stimulated with a 100 mM K^+ solution (Black line on each trace). g) schematic representation of mean spikes obtained from those recordings. h)–j) violin plots representing respectively the number of exocytotic events, spike time to peak and feet duration of individual spikes (Bars in the plot represent from top to bottom, third quartile, median and first quartile). ns: non-significant, ****: $p < 0.0001$, Kruskall–Wallis followed by Dunn's multiple comparisons test versus control ($N > 82$ per condition from three independent cultures), other parameters were also quantified and yielded similar results (FigureSI 18).

 © 2025 The Author(s). Angewandte Chemie International Edition published by Wiley-VCH GmbH

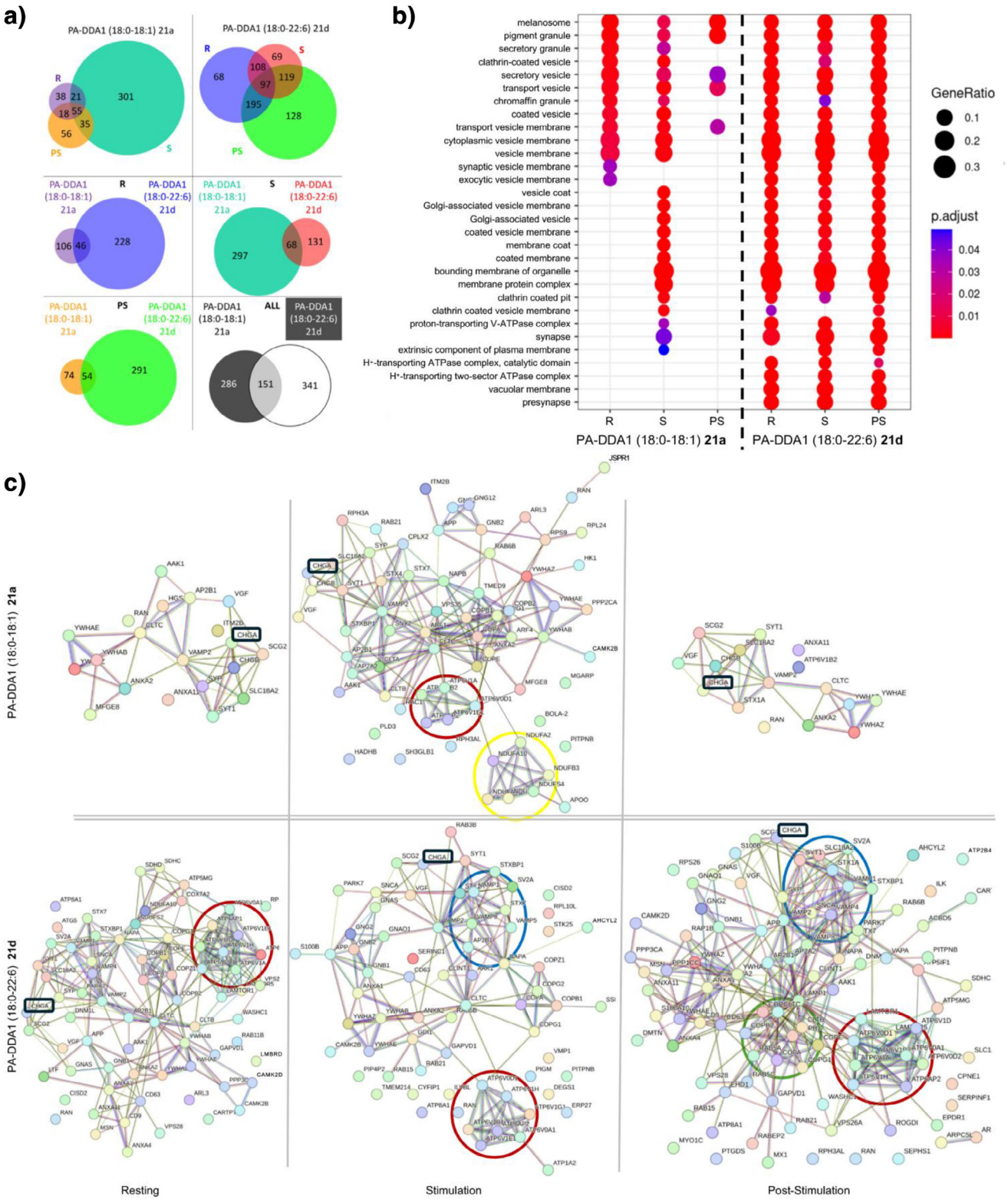

Figure 6. PA interactome in neurosecretory cells. a) distribution of different proteins identified in the fishing experiments performed in bovine chromaffin cells for PA-DDA1 (18:0–18:1) **21a** and PA-DDA1 (18:0–22:6) **21d** in resting condition (R), stimulated condition S), or resting condition post-stimulation (PS). b) cellular component of Gene Ontology enrichment analysis of all proteins identified in the different tested conditions. Biological process, Molecular function, and KEGG Gene Ontology analysis are shown on FigureSI 21. c) Protein–Protein Interaction Network Exploration of the pooled proteins identified in the cellular component Gene Ontology enrichment analysis for potential PA interactors under different conditions using Cytoscape (STRING data base). Circles highlight clusters of proteins involved in interactions: red (H^+ transport by V-ATPase), blue (SNAREs), yellow (mitochondrial activity), green (membrane coats).

© 2025 The Author(s). Angewandte Chemie International Edition published by Wiley-VCH GmbH

biological processes. These tools can be applied to study lipid signaling dysregulation in neurodegenerative diseases by tracking PA species in neurons or glial cells, and to investigate how specific PAs modulate membrane curvature and trafficking in cancer cells or during organelle remodeling.[54] Additionally, clickable moieties enable the identification of novel PA-binding proteins through chemoproteomics, offering insights into lipid–protein interaction networks altered in metabolic disorders. Overall, this platform enables precise mechanistic studies of GPL-mediated signaling, with potential implications for therapeutic targeting in diverse pathologies.

Conclusion

This work provides access to patented versatile and clickable PA analogues, that preserve natural fatty acyl chains and the phosphate headgroup, thus confirming their potential for *in cellulo* applications.[55] Unlike currently commercially available PA analogues, modified on their fatty acyl chains, these synthetic analogues faithfully reproduce the biological behavior of natural lipids. This highlights importance of fatty acyl chain composition for biological studies involving PA and probably other GPLs. Finally, fishing experiments performed on primary cells not only confirmed known interactions but also revealed dozens of others unknown interactions, depending both on the fatty acyl chain and the cellular state. Overall, these novel synthetic GPL significantly broaden our knowledge of PA partners and functions, opening new avenues for exploring lipid-mediated cellular processes such as membrane curvature regulation, lipid signaling dysregulation in neurodegenerative disease, or cancer and from a more fundamental manner the lipid interactome.

Supporting Information

The authors have cited additional references within the Supporting Information.[56,65]

Acknowledgements

This work was supported by grants from "Fondation pour la Recherche Médicale" (DEI20151234424) and "Agence Nationale pour la Recherche" (ANR-19-CE44-0019) to NV, PYR, SB and MM-H, " Fondation pour la Recherche Médicale " (FDT202304016618) to AW, French Proteomic Infrastructure (ProFI; ANR-10-INBS-08–03) to JMS. INSERM is providing the salary to N.V. and S.G. T.F. and F.L. are co-supported by European Union and Région Normandie. This work has been partially supported by Université Rouen Normandie, INSA Rouen Normandie, Centre National de la Recherche Scientifique (CNRS), European Regional Development Fund (ERDF), Labex SynOrg (ANR-11-LABX-0029), Carnot Institute I2C, and the graduate school for research XL-Chem (ANR-18-EURE-0020 XL CHEM).

The authors acknowledge the In Vitro Imaging Platform – NeuroPôle – Strasbourg (UAR3156), member of the national infrastructure France-BioImaging supported by the French National Research Agency (ANR-10-INBS-04).

The authors acknowledge the municipal slaughterhouse of Haguenau (France) and the slaughterhouse of Bigard Formerie (France) for providing the bovine adrenal glands.

The authors acknowledge the members of the Plateforme C2I Orga, specifically Laetitia Bailly, Emily Petit, Albert Marccual, Mathilde Lauzent and Françoise Ringot.

S.B. thanks Dr. Antoine Joosten and Dr. Alexandre Haefelé for the scientific discussions about this project.

Conflict of Interests

The authors declare no conflict of interest.

Data Availability Statement

The data that support the findings of this study are available in the Supporting Information of this article.

Keywords: Click chemistry • Exocytosis • Phospholipids • Photolabelling • Probes design

[1] C. Schultz, *Acc. Chem. Res.* **2023**, *56*, 1168–1177.
[2] J. M. Punt, D. van der Vliet, M. van der Stelt, *Acc. Chem. Res.* **2022**, *55*, 3205–3217.
[3] K. Yang, X. Han, *Trends Biochem. Sci.* **2016**, *41*, 954–969.
[4] Y. V. Shulga, D. S. Myers, P. T. Ivanova, S. B. Milne, H. A. Brown, M. K. Topham, R. M. Epand, *Biochemistry* **2010**, *49*, 312–317.
[5] A. Y. Andreyev, E. Fahy, Z. Guan, S. Kelly, X. Li, J. G. McDonald, S. Milne, D. Myers, H. Park, A. Ryan, B. M. Thompson, E. Wang, Y. Zhao, H. A. Brown, A. H. Merrill, C. R. Raetz, D. W. Russell, S. Subramaniam, E. A. Dennis, *J. Lipid Res.* **2010**, *51*, 2785–2797.
[6] T. G. Oliveira, R. B. Chan, H. Tian, M. Laredo, G. Shui, A. Staniszewski, H. Zhang, L. Wang, T.-W. Kim, K. E. Duff, M. R. Wenk, O. Arancio, G. D. Paolo, *J. Neurosci.* **2010**, *30*, 16419–16428.
[7] J. Klein, *J. Neurochem.* **2005**, *94*, 1473–1487.
[8] U. Burkhardt, B. Wojcik, M. Zimmermann, J. Klein, *Neuropharmacology* **2014**, *79*, 1–9.
[9] M. H. Park, B.-H. Ahn, Y.-K. Hong, D. S. Min, *Carcinogenesis* **2009**, *30*, 356–365.
[10] R. Tabet, E. Moutin, J. A. J. Becker, D. Heintz, L. Fouillen, E. Flatter, W. Krężel, V. Alunni, P. Koebel, D. Dembélé, F. Tassone, B. Bardoni, J.-L. Mandel, N. Vitale, D. Muller, J. Le Merrer, H. Moine, *Proc. Natl. Acad. Sci. USA* **2016**, *113*, E3619–E3628.
[11] M.-R. Ammar, Y. Humeau, A. Hanauer, B. Nieswandt, M.-F. Bader, N. Vitale, *J. Neurosci.* **2013**, *33*, 19470–19479.
[12] C. M. Metrick, E. A. Peterson, J. C. Santoro, I. J. Enyedy, P. Murugan, T. Chen, K. Michelsen, M. Cullivan, K. A. Spilker, P. R. Kumar, T. L. May-Dracka, J. V. Chodaparambil, *Nat. Chem. Biol.* **2020**, *16*, 391–399.
[13] F. Z. Bowling, C. M. Salazar, J. A. Bell, T. S. Huq, M. A. Frohman, M. V. Airola, *Nat. Chem. Biol.* **2020**, *16*, 400–407.
[14] E. Tanguy, N. Kassas, N. Vitale, *Biomolecules* **2018**, *8*, 20.
[15] A. Rizzo, K. Shome, S. C. Watkins, G. Romero, *J. Biol. Chem.* **2000**, *275*, 23911–23918.
[16] M. A. Frias, A. Hatipoglu, D. A. Foster, *Trends Endocrinol. Metab.* **2023**, *34*, 170–180.

© 2025 The Author(s). Angewandte Chemie International Edition published by Wiley-VCH GmbH

[17] S. Schrecke, Y. Zhu, J. W. McCabe, M. Bartz, C. Packianathan, M. Zhao, M. Zhou, D. Russell, A. Laganowsky, *Nat. Chem. Biol.* **2021**, *17*, 89–95.
[18] P.-H. B. Chen, X.-L. Li, J. M. Baskin, *Chem. Rev.* **2025**, *125*, 2502–2560.
[19] P. A. M. M. Varandas, A. J. A. Cobb, M. A. Segundo, E. M. P. Silva, *Bioconjugate Chem.* **2020**, *31*, 417–435.
[20] Ł. Joachimiak, K. M. Błażewska, *J. Med. Chem.* **2018**, *61*, 8536–8562.
[21] J. Greaves, K. R. Munro, S. C. Davidson, M. Riviere, J. Wojno, T. K. Smith, N. C. O. Tomkinson, L. H. Chamberlain, *Proc. Natl. Acad. Sci. USA* **2017**, *114*, E1365–E1374.
[22] W. Diakowski, Ł. Ozimek, E. Bielska, S. Bem, M. Langner, A. F. Sikorski, *Biochim. Biophys. Acta – Biomembr.* **2006**, *1758*, 4–12.
[23] G. van Meer, D. R. Voelker, G. W. Feigenson, *Nat. Rev. Mol. Cell Biol.* **2008**, *9*, 112–124.
[24] B. Wang, P. Tontonoz, *Annu. Rev. Physiol.* **2019**, *81*, 165–188.
[25] E. Salnikov, B. Bechinger, *Biochim. Biophys. Acta – Biomembr.* **2022**, *1864*, 184001.
[26] B. A. Smith, E. J. O'Neil, A. J. Lampkins, J. R. Johnson, J.-J. Lee, E. L. Cole, B. D. Smith, *J. Fluoresc.* **2012**, *22*, 93–101.
[27] M. D. Smith, C. G. Sudhahar, D. Gong, R. V. Stahelin, M. D. Best, *Mol. BioSyst.* **2009**, *5*, 962.
[28] A. Holý, *Synthesis* **1998**, *1998*, 381–385.
[29] L. Y. Chan, S. Kim, T. Ryu, P. H. Lee, *Chem. Commun.* **2013**, *49*, 4682.
[30] M. F. Gordeev, D. V. Patel, P. L. Barker, E. M. Gordon, *Tetrahedron Lett.* **1994**, *35*, 7585–7588.
[31] Y. Yamamoto, T. Itoh, K. Yamamoto, *Org. Biomol. Chem.* **2017**, *15*, 8186–8192.
[32] L. M. Gaetke, C. K. Chow, *Toxicology* **2003**, *189*, 147–163.
[33] J. Garcia-Hartjes, J. Dommerholt, T. Wennekes, F. L. van Delft, H. Zuilhof, *Eur. J. Org. Chem.* **2013**, *2013*, 3712–3720.
[34] A. Kuzmin, A. Poloukhtine, M. A. Wolfert, V. V. Popik, *Bioconjugate Chem.* **2010**, *21*, 2076–2085.
[35] E. Tanguy, P. Costé De Bagneaux, N. Kassas, M.-R. Ammar, Q. Wang, A.-M. Haeberlé, J. Raherindratsara, L. Fouillen, P.-Y. Renard, M. Montero-Hadjadje, S. Chasserot-Golaz, S. Ory, S. Gasman, M.-F. Bader, N. Vitale, *Cell Rep.* **2020**, *32*, 108026.
[36] Q. Ibert, M. Cauwel, T. Glachet, T. Tite, P. Le Nahenec-Martel, J.-F. Lohier, P.-Y. Renard, X. Franck, V. Reboul, C. Sabot, *Adv. Synth. Catal.* **2021**, *363*, 4390–4398.
[37] M.-F. Bader, R. W. Holz, K. Kumakura, N. Vitale, *Ann N-Y Acad Sci* **2002**, *971*, 178–183.
[38] M.-F. Bader, N. Vitale, *Biochim. Biophys. Acta, Mol. Cell Biol. Lipids* **2009**, *1791*, 936–941.
[39] E. Tanguy, A. Wolf, Q. Wang, S. Chasserot-Golaz, S. Ory, S. Gasman, N. Vitale, *Adv. Biol. Regul.* **2022**, *83*, 100844.
[40] N. Kassas, E. Tanguy, T. Thahouly, L. Fouillen, D. Heintz, S. Chasserot-Golaz, M.-F. Bader, N. J. Grant, N. Vitale, *J. Biol. Chem.* **2017**, *292*, 4266–4279.
[41] O. Carmon, F. Laguerre, L. Riachy, C. Delestre-Delacour, Q. Wang, E. Tanguy, L. Jeandel, D. Cartier, T. Thahouly, A.-M. Haeberlé, L. Fouillen, O. Rezazgui, D. Schapman, A. Haefelé, Y. Goumon, L. Galas, P.-Y. Renard, S. Alexandre, N. Vitale, Y. Anouar, M. Montero-Hadjadje, *FASEB J.* **2020**, *34*, 6769–6790.
[42] J. Bigay, B. Antonny, *Dev. Cell* **2012**, *23*, 886–895.
[43] E. Asuncion-Punzalan, K. Kachel, E. London, *Biochemistry* **1998**, *37*, 4603–4611.
[44] S. Chasserot-Golaz, J. R. Coorssen, F. A. Meunier, N. Vitale, *Cell. Mol. Neurobiol.* **2010**, *30*, 1335–1342.
[45] E. Tanguy, Q. Wang, N. Vitale, in *Lipid Signaling in Human Diseases* (Eds.: J. Gomez-Cambronero, M. A. Frohman), Springer International Publishing, Cham, **2020**, pp. 115–130. https://doi.org/10.1007/164_2018_180.
[46] M. Manifava, J. W. J. F. Thuring, Z.-Y. Lim, L. Packman, A. B. Holmes, N. T. Ktistakis, *J. Biol. Chem.* **2001**, *276*, 8987–8994.
[47] R. E. Kattan, H. Han, G. Seo, B. Yang, Y. Lin, M. Dotson, S. Pham, Y. Menely, W. Wang, *Mol. Cell. Proteomics* **2022**, *21*, 100195.
[48] H. Zhou, Y. Huo, N. Yang, T. Wei, *The FEBS Journal* **2024**, *291*, 1870–1885.
[49] J. Zegarlińska, M. Piaścik, A. F. Sikorski, A. Czogalla, *Acta Biochim. Pol.* **2018**, *65*, 163–171.
[50] M. A. Zhukovsky, A. Filograna, A. Luini, D. Corda, C. Valente, *FEBS Lett.* **2019**, *593*, 2428–2451.
[51] Q. Wang, A. Wolf, S. Ozkan, L. Richert, Y. Mely, S. Chasserot-Golaz, S. Ory, S. Gasman, N. Vitale, *Front. Mol. Biosci.* **2023**, *10*, 1163545.
[52] A. D. Lam, P. Tryoen-Toth, B. Tsai, N. Vitale, E. L. Stuenkel, *Mol. Biol. Cell* **2008**, *19*, 485–497.
[53] D. W. Kang, K.-Y. Choi, D. S. Min, *J. Biol. Chem.* **2014**, *289* 22575–22582.
[54] H. A. Brown, P. G. Thomas, C. W. Lindsley, *Nat Rev Drug Discov* **2017**, *16*, 351–367.
[55] S. Balieu, P.-Y. Renard, M. Montero-Hadjaje, N. Vitale, A. Cocq, A. Schlichter, R. Ferlet, A. Haefelé, L. Riachy, A. Wolf, *FR20220002640*, CNRS; Université de Rouen-Normandie; INSA de Rouen Normandie; INSRM, France, **2022**.
[56] N. Nagashima, M. Ohno, *Chem. Phar. Bull.* **1991**, *39*, 1972–1982.
[57] J.-C. Namyslo, R. Schaefer, M. E. Maier, *ChemInform* **1999**, *30*. https://doi.org/10.1002/chin.199946228.
[58] R. S. Ghogare, S. B. Wadavrao, A. V. Narsaiah, *Helv. Chim. Acta* **2016**, *99*, 247–254.
[59] C. X. Liu Ningning, Z. Qingshan, W.u Qinpei, *Chinese Journal of Organic Chemistry* **2014**, *34*, 1364–1368.
[60] K. Nakayama, J. D. Rainier, *Tetrahedron* **1990**, *46*, 4165–4170.
[61] A. Chevalier, C. Massif, P.-Y. Renard, A. Romieu, *Chem.-Eur. J.* **2013**, *19*, 1686–1699.
[62] S. Poëa-Guyon, M. R. Ammar, M. Erard, M. Amar, A. W. Moreau, P. Fossier, V. Gleize, N. Vitale, N. Morel, *J. Cell Biol.* **2013**, *203*, 283–298.
[63] D. Bouyssié, A.-M. Hesse, E. Mouton-Barbosa, M. Rompais, C. Macron, C. Carapito, A. Gonzalez de Peredo, Y. Couté, V. Dupierris, A. Burel, J.-P. Menetrey, A. Kalaitzakis, J. Poisat, A. Romdhani, O. Burlet-Schiltz, S. Cianférani, J. Garin, C. Bruley, *Bioinformatics (Oxford, England)* **2020**, *36*, 3148–3155.
[64] G. Yu, L. G. Wang, Y. Han, Q. Y. He, *OMICS* **2012**, *16*, 284–287.
[65] T. Wu, E. Hu, S. Xu, M. Chen, P. Guo, Z. Dai, T. Feng, L. Zhou, W. Tang, L. Zhan, X. Fu, S. Liu, X. Bo, G. Yu, *Innovation (Camb)* **2021**, *2*, 100141.

Manuscript received: May 12, 2025
Revised manuscript received: July 02, 2025
Accepted manuscript online: July 04, 2025
Version of record online: July 25, 2025

© 2025 The Author(s). Angewandte Chemie International Edition published by Wiley-VCH GmbH